Available online at www.sciencedirect.com
ScienceDirect
C. R. Geoscience 341 (2009) 439–445
COMPTES RENDUS GEOSCIENCE

Internal geophysics

# Inner core structure: Constraints from frequency dependent seismic anisotropy

Annie Souriau

*CNRS, Observatoire Midi-Pyrénées, 14, avenue Edouard-Belin, 31400 Toulouse, France*

Received 17 March 2009; accepted after revision 22 April 2009
Available online 13 June 2009

Presented by Annie Cazenave

**Abstract**

Seismic waves sampling the inner core have revealed that it is anisotropic, propagation being faster and attenuation stronger for waves travelling parallel to the Earth's rotation axis, relative to those parallel to the equatorial plane. Here, the anisotropy in attenuation is investigated in the frequency range 0.2–2 Hz, in a region of the uppermost inner core sampled by rays of various orientations. A spectacular amplitude decay with frequency is observed for polar paths whereas it is very mild for equatorial paths, leading to a much stronger anisotropy at high frequency than at low frequency. A velocity dispersion is also observed for polar paths, with a propagation faster at high frequency than at low frequency. These observations may provide important constraints on the texture of the inner core, and help to better understand its growth mechanism. ***To cite this article: A. Souriau, C. R. Geoscience 341 (2009).***


**Résumé**

**Structure du noyau interne : contraintes données par les variations de l'anisotropie avec la fréquence.** Les ondes sismiques qui traversent le noyau interne solide de la terre (ou graine) ont montré qu'il a une structure anisotrope, aussi bien pour les vitesses que pour l'atténuation : les ondes se propageant parallèlement à l'axe de rotation de la terre sont plus rapides et plus atténuées que celles se propageant parallèlement au plan équatorial. On montre ici que cet effet est fortement dépendant de la fréquence. L'anisotropie d'atténuation est étudiée dans la gamme de fréquences 0.2–2 Hz, pour des rais échantillonnant la partie supérieure de la graine avec différentes orientations dans une région donnée. Une décroissance spectaculaire de l'amplitude des ondes avec la fréquence est observée pour les trajets polaires, alors que cette décroissance reste faible pour les trajets équatoriaux. En conséquence, l'anisotropie de la graine apparaît beaucoup plus forte à haute fréquence qu'à basse fréquence. Parallèlement, une forte dispersion est observée pour les trajets polaires, avec une propagation plus rapide à haute fréquence qu'à basse fréquence. Ces observations peuvent apporter d'importantes contraintes sur la texture de la graine et donc contribuer à mieux comprendre le mécanisme de sa croissance. ***Pour citer cet article : A. Souriau, C. R. Geoscience 341 (2009).***


*Keywords:* Core; Inner core; Attenuation; Anisotropy; Dispersion; PKP waves

*Mots clés :* Noyau ; Graine ; Atténuation ; Anisotropie ; Dispersion ; Ondes PKP

*E-mail address:* Annie.Souriau@dtp.obs-mip.fr.

1631-0713/$ – see front matter 
doi:10.1016/j.crte.2009.04.006

## 1. Introduction

The solid inner core is one of the most puzzling parts of our planet. Its structure is principally constrained by the propagation of the compressional waves PKPdf (also called PKIKP), which have revealed that the inner core is anisotropic both in seismic velocities [20] and attenuation [28]. Propagation is faster and attenuation is stronger for waves propagating parallel to the Earth's rotation axis (hereafter denoted ''polar paths''), than for waves parallel to the equatorial plane (hereafter denoted ''equatorial paths'') [8,11,17,22,34]. P-velocity is 1 to 3% faster for polar paths than for equatorial paths, a result confirmed by the analysis of the free oscillations of the Earth (see review, [25]). This observation is generally ascribed to a preferred orientation of anisotropic crystals of iron in hexagonal compact form or other forms stable at core conditions. The anisotropy is not uniform: the uppermost 100 km are nearly isotropic at worldwide scale [29], and a different form of anisotropy is present in the central part [3,15]. Moreover, a hemispherical pattern has been detected [12,32], the western hemisphere being more anisotropic than the eastern one, a pattern possibly induced by liquid core dynamics [1,30]. In parallel to velocity anisotropy, an anisotropy in attenuation has been observed, high attenuation being related to fast propagation [8,11,17,22,34]. This correlation is opposite to that in the mantle, where viscous attenuation due to thermal heterogeneities is dominant [23]. Viscous attenuation, which implies conversion of seismic energy into heat, is likely to be present in the inner core [10,17], in particular if partially molten material is present [19,24]. However, wave scattering by the inner core texture seems a preferred mechanism to explain the observed velocity-attenuation correlation [10,11]. The identification of scatterers in the uppermost inner core [33] gives additional credit to this hypothesis, but elements are missing to characterize their relative contribution to attenuation.

It is of major interest to specify the structure of the uppermost inner core, in order to understand its growth mechanism through crystallization of the liquid outer core. As attenuation is more sensitive than velocity to the structure properties, attention has been primarily focussed on wave amplitudes.

## 2. Data

Events of magnitude $M \geq 6.0$ sampling a small region of the inner core beneath Africa have been selected in the period 1986–2008, providing PKPdf rays with many different orientations at their turning points (Fig. 1). The data are vertical broadband records. The distance range is limited to 149–152°, which gives turning points 200 to 300 km beneath the inner core boundary (ICB). In the selected distance range, it is possible to compare PKPdf with another core phase, PKPbc, which turns in the liquid core and has a nearby path (Fig. 2a). Most of the source effects and propagation perturbations through the mantle are thus eliminated in the PKPdf/PKPbc amplitude ratio (hereafter noted *DF/BC*). The only remaining contribution is the propagation of PKPdf through the inner core, as the liquid core is laterally homogeneous and has a very low attenuation [9].

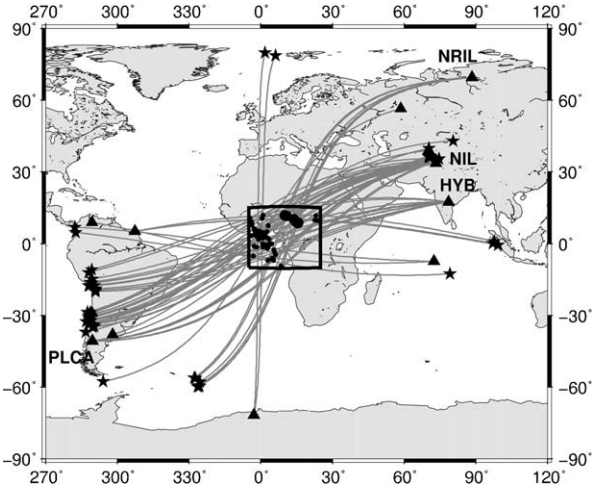


Fig. 1. Selected paths with various orientations with respect of Earth rotation axis, and turning points beneath Africa (box). Stations with codes are those used in Fig. 3 and 4.

Fig. 1. Trajets étudiés, avec le point le plus bas sous l'Afrique (cadre) et différentes orientations par rapport à l'axe de rotation de la terre. Les stations avec des codes sont celles utilisées dans les Fig. 3 et 4.

Each PKPdf ray is characterized by its ray parameter, which is directly related to its turning depth, and which is fully determined from the epicentral distance $\Delta$, focal depth $h$ and Earth's model. The PKPdf ray parameters of the selected data range from $p = 1.50$ s/deg (for $\Delta = 152°$ and $h = 0$) to $p = 1.61$ s/deg (for $\Delta = 149°$ and $h = 0$). The reference velocity model is ak135 [16], which is presently the best core model for compressional body waves. In particular, it exhibits a low velocity gradient at the base of the liquid core which correctly reproduces the propagation times and amplitudes of PKPbc. As this model does not provide attenuation parameters, the quality factor $Q$ of model PREM [14] is used. It is mostly constrained from eigenmodes. The $Q$-model in the mantle has only a

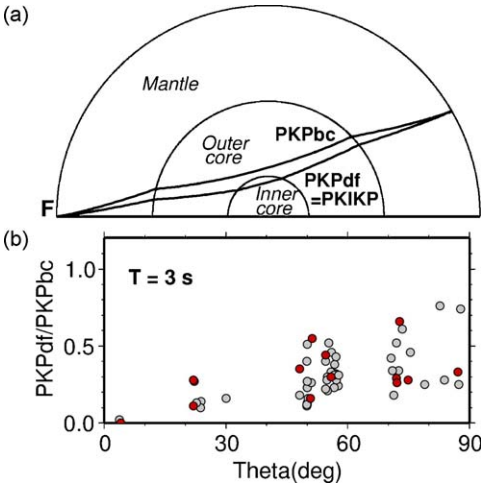


Fig. 2. **a:** ray paths of PKPdf and PKPbc inside the Earth at distance 150°; PKPbc is the reference phase; **b:** amplitude ratio PKPdf/PKPbc as a function of $\theta$, the angle of the PKPdf ray with respect to Earth rotation axis, at period 3 s. The amplitude ratios have been corrected for distance $\Delta$ and focal depth (red dots [darker dots] for $\Delta > 151°$ to check a possible influence of PKPbc diffraction at ICB). Note the anisotropy in PKPdf amplitude, with a strong attenuation for paths parallel to Earth rotation axis.

Fig. 2. **a :** trajets des rais PKPdf et PKPbc dans la Terre, à la distance de 150°; PKPbc sert de référence ; **b :** rapport des amplitudes PKPdf/PKPbc à la période de trois secondes, en fonction de l'angle $\theta$ entre le rai et l'axe de rotation de la Terre. Les valeurs sont corrigées de l'influence de la distance $\Delta$ et de la profondeur du foyer (points rouges [plus foncés] pour les rais susceptibles d'être perturbés par la diffraction, $\Delta > 151°$). On observe l'anisotropie d'atténuation de PKPdf, avec une forte atténuation pour les trajets parallèles à l'axe de rotation de la Terre.

marginal influence, as the *DF/BC* ratio will be considered.

Before investigating any frequency dependence, it has first to be checked that an anisotropy in attenuation is effectively observed, as in previous studies [8,11,17,22,34]. The experimental ratios *DF/BC* are determined at period 3 s. A ray-parameter correction equivalent to a distance-focal depth correction is determined using synthetic seismograms computed using the reflectivity method [21] for the reference model. It is applied to the experimental ratios, to refer all the data to the value $p = 1.6$ s/deg. Despite a strong data scattering likely due to lower mantle heterogeneities, the corrected *DF/BC* ratios (Fig. 2b) clearly show a decrease for small ray angle $\theta$ with respect to the Earth's rotation axis, with values close to zero for two quasi-polar paths. Note that no perturbing effect of the diffraction of PKPbc at ICB may be observed for the large distances (red dots on Fig. 2b). The *DF/BC* variations of more than one order of magnitude thus confirm the existence of an anisotropy in attenuation.

## 3. The frequency dependence of wave amplitudes: method and observations

Important information may be given by the variations of *DF/BC* with frequency $f$. If the quality factor $Q$ is not frequency dependent, Ln*(DF/BC)* decreases linearly with increasing frequency [6,27] with slope $-\pi * t_{ic}/Q$, $t_{ic}$ being the time spent by PKPdf inside the inner core. This may occur if attenuation is characterized by a broad absorption band with constant $Q$ resulting from the superposition of multiple viscous mechanisms [18], as postulated in PREM [14]. On the other hand, scattering attenuation occurs when the waves meet heterogeneities of scale length close to their wavelength, so that some energy is deflected outside the source-station direction. In this case, attenuation becomes generally frequency dependent with a dependence which reflects the heterogeneity spectrum. Attenuation may become maximum at a particular frequency, if heterogeneities have a prevailing wavelength [7,11]. Ln*(DF/BC)* is generally no longer a linear function of $f$ and may exhibit a strong frequency dependence [11].

The variations of Ln(*DF/BC*) with frequency are examined in the frequency range 0.2–2.0 Hz for the data of Fig. 1. Note that the highest frequencies have rarely been explored for core studies, but that $Q$ in the reference model is defined at low frequencies (about two orders lower than those considered here). The investigated frequency domain is restricted at the low-frequency side by the time delay between PKPdf and PKPbc (Fig. 3a, b). Moreover, large magnitude events with long time duration must be eliminated, because PKPdf may overlap PKPbc and biases the PKPdf/PKPbc amplitude ratio (it turns out that no such event was present in our initial selection, for paths turning beneath Africa). At high frequency, the spectral domain is limited by the noise level. Records are band-pass filtered at 20 different frequency values $f_0$ (frequency bands from $0.6*f_0$ to $1.4*f_0$), with causal Butterworth filters to avoid perturbation of the low amplitude PKPdf signal by the large amplitude PKPbc wave. Measurements of *DF/BC* have been made automatically on the filtered data. Two methods have been checked: *1-* compute the cross-correlation of the signal selected inside the PKPdf and PKPbc windows, *2-* compute the ratios of the peak-to-peak maximum amplitudes. In each case, the windows are defined by taking into account the time shift due to filtering, and for PKPdf the influence of velocity anisotropy. The two methods give globally similar results, the second one gives generally more stable results and has been adopted.

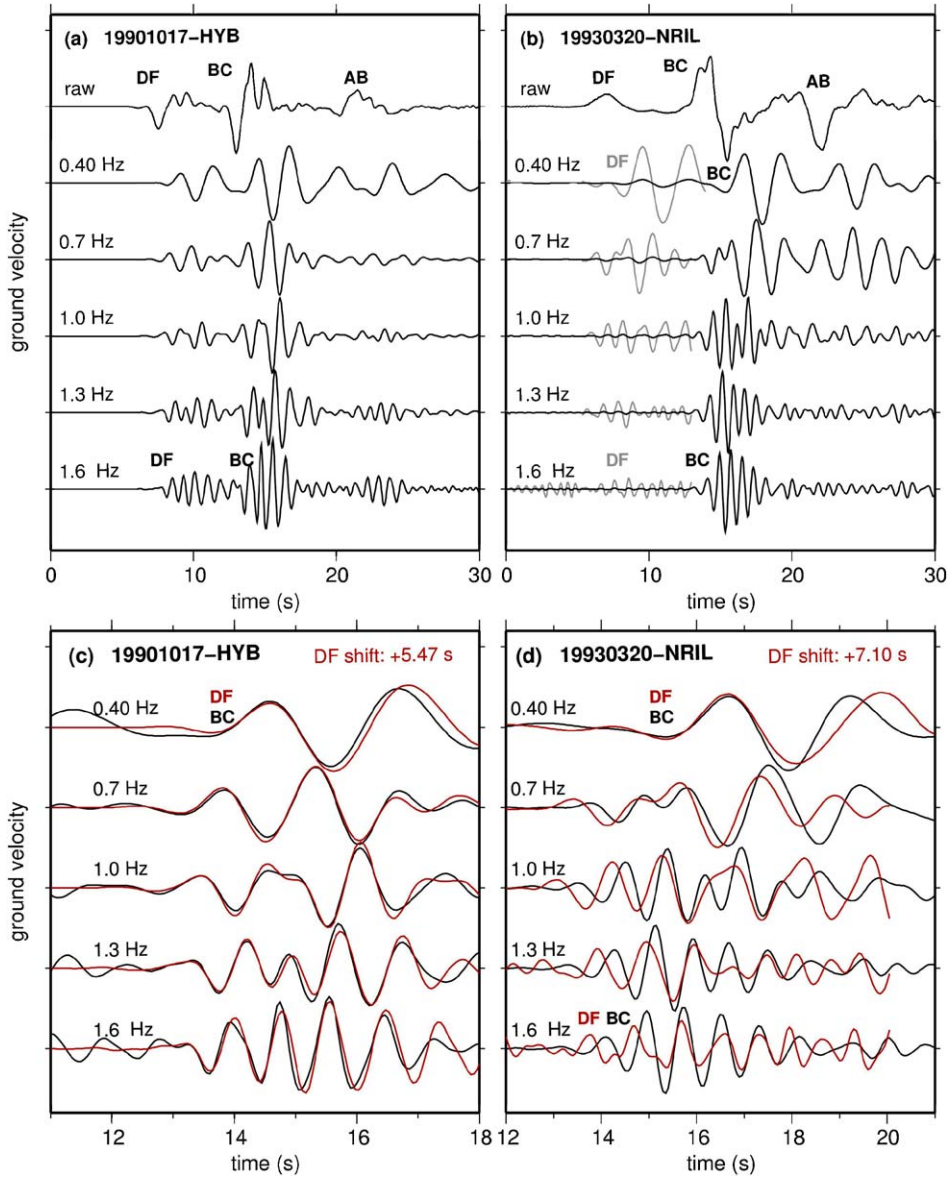


Fig. 3. Vertical components of two events with turning points beneath Africa, with raw data and data bandpass filtered at different frequencies. **a:** quasi-equatorial path (October 17, 1990 recorded at HYB, distance 149.6°, depth 599 km, angle to Earth rotation axis ∼73°); **b:** quasi-polar path (March 20, 1993 recorded at NRIL, distance 149.6°, depth 116 km, angle to Earth rotation axis ∼23°). The three core phases are well observed: DF = PKPdf, which samples the inner core, BC = PKPbc and AB = PKPab which turn at the base and in the middle of the liquid core, respectively. Traces are scaled to the PKPbc amplitude. The time shift on the filtered traces is due to the causal filtering. In (b), grey traces correspond to the signal enhanced by a factor of 10. Note the mild decrease of the PKPdf amplitude with increasing frequency for the equatorial path, and its very strong decrease for the polar path; **c, d**: close-up on the PKPbc phase for filtered traces (in black), and PKPdf scaled to the PKPbc amplitude (in red [lighter line]) and shifted in time of a constant value to be superimposed to PKPbc at 0.4 Hz. A dispersion is clearly observed for the quasi-polar path.

Fig. 3. Composantes verticales de deux enregistrements ayant leur point le plus bas sous l'Afrique, avec les données brutes (en haut) et filtrées à différentes fréquences. **a** : trajet quasi-équatorial (séisme du 17 octobre 1990 enregistré à HYB, distance 149,6°, profondeur de foyer 599 km, angle du rai ∼73° par rapport à l'axe de rotation de la Terre) ; **b** : trajet quasi-polaire (séisme du 20 mars 1993 enregistré à NRIL, distance 149,6°, profondeur du foyer 116 km, angle du rai ∼23° par rapport à l'axe de rotation de la Terre). On observe les trois phases du noyau : DF = PKPdf qui échantillonne la graine, BC = PKPbc et AB = PKPab qui échantillonnent respectivement la base et le milieu du noyau liquide. PKPbc sert de référence. Le décalage temporel des différentes traces est dû au filtre causal, les traces grises (en b) sont multipliées par un facteur 10. On note la décroissance lente de l'amplitude de PKPdf avec la fréquence pour les trajets équatoriaux et sa décroissance très rapide pour les trajets polaires ; **c, d** : zoom sur les traces filtrées, PKPbc (en noir) et PKPdf (en rouge [traces plus claires]) ramené à la même amplitude et décalé en temps d'une valeur constante pour que les traces soient superposées à 0,4 Hz. Une dispersion est clairement observée pour le trajet quasi polaire.

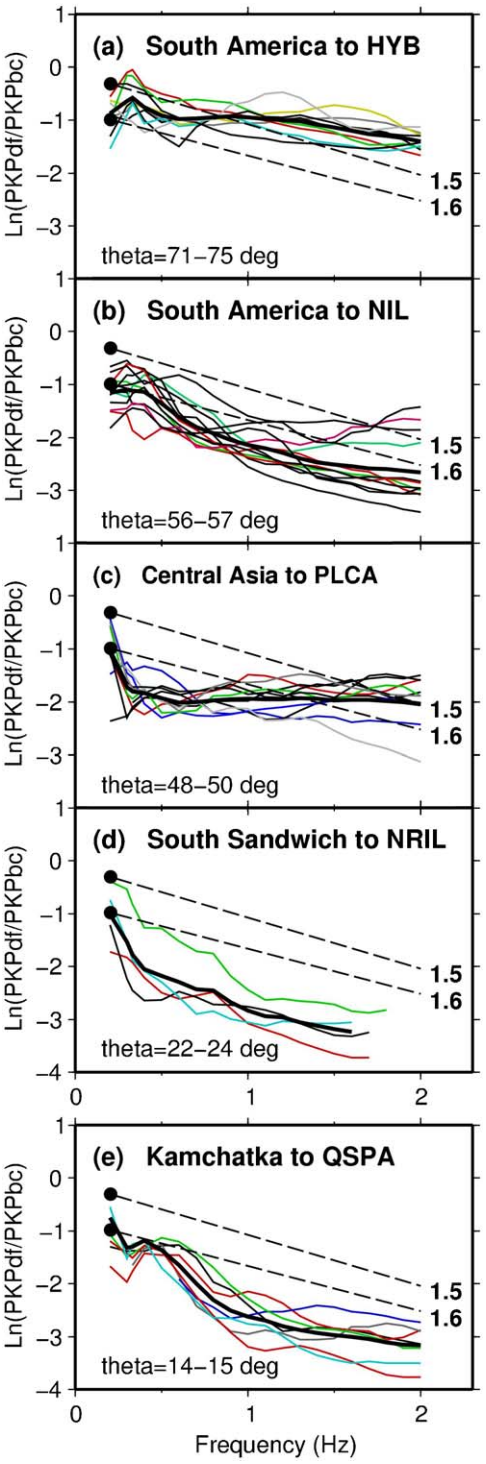


Fig. 4. Amplitude ratio *DF/BC* as a function of frequency for selected paths turning beneath Africa, with decreasing values of the angle $\theta$ of the ray with respect to Earth rotation axis. **a**: quasi-equatorial paths; **b, c**: intermediate $\theta$-values; **d**: quasi-polar paths; **e**: results for another polar path with turning point beneath Western Pacific. In each figure, each thin curve corresponds to a record, and the thick black curve corresponds to the mean. The two black dots correspond to the theoretical values for the mean reference model (see text) for two values of the ray parameter (1.5 and 1.6), and the two dashed lines are the expected values if $Q$ is not frequency dependent. Note the drastic influence of the $\theta$-value, the departure from linearity and the strong amplitude decay at high frequency for polar paths.

Fig. 4. Rapport d'amplitude *DF/BC* en fonction de la fréquence pour différents trajets ayant leur point le plus bas sous l'Afrique, et pour des valeurs décroissantes de l'angle $\theta$ entre le rai et l'axe de rotation de la Terre. **a** : trajets quasi équatoriaux ; **b, c** : valeurs intermédiaires de $\theta$ ; **d** : trajets quasi polaires ; **e** : résultats pour un autre trajet polaire avec un point le plus bas sous le Pacifique ouest. Pour chaque figure, chaque courbe fine correspond à un enregistrement ; la courbe noire épaisse correspond à la moyenne. Les deux points noirs correspondent aux valeurs théoriques du modèle moyen de référence (voir texte) pour deux valeurs de paramètre de rai (1,5 et 1,6). Les deux droites pointillées sont les valeurs attendues, si Q ne dépend pas de la fréquence. On note l'influence très importante de $\theta$, l'écart à la linéarité, et la forte décroissance des amplitudes à haute fréquence pour les trajets polaires.

Fig. 3a, b shows two examples of filtered records, for a nearly equatorial path and a nearly polar path. They confirm the anisotropy in attenuation, but they also reveal a drastic difference in amplitude decay with frequency between the two paths. Fig. 3c, d focus on the time delay between PKPdf and PKPbc. The elastic anisotropy is well observed: The time delay between PKPdf and PKPbc is 5.47 s for the quasi-equatorial path, 7.10 s for the quasi-polar path at 0.4 Hz, which results in a difference of 2.1 s after correction of epicentral distances and focal depths. This corresponds to an anisotropy of about 2%. A strong dispersion is also observed for polar paths, the PKPdf propagation being about 0.36 s faster at 1.6 Hz than at 0.4 Hz. Such a dispersion is not observed for the equatorial path**.** It is quite unusual to observe such a large dispersion for body waves. The dispersion is linked to attenuation, PREM isotropic model with $Q \sim 440$ predicts a time shift of only 0.13 s. Theoretical models show that dispersion curves may give strong constraints on the attenuation mechanisms [11,17,18]. Unfortunately, absolute measurements of dispersion are not possible here, so that dispersion will not be further considered.

## 4. Amplitude spectra for various ray orientations

Fig. 4 gives the amplitude ratios as a function of frequency for four, well sampled paths, which correspond to different $\theta$-values. Also reported are the values obtained from synthetic seismograms at 0.2 Hz for the reference model ($Q = 440$ in the uppermost inner core) for two ray parameters

($p = 1.5$ and 1.6 s/deg), and the linear variations expected if $Q$ is independent of frequency. For the quasi-equatorial paths from South America to HYB, India ($\theta \sim 73^\circ$, Fig. 4a), the variation of Ln(*DF/BC*) with $f$ is nearly linear, supporting a model of viscous attenuation with constant $Q$. The results agree with the predictions of the mean Earth model ($Q = 440$) at the low frequency side, but the slope gives a higher $Q$-value ($Q \sim 800$–$1200$), an inconsistency which suggests that different mechanisms may contribute to attenuation, depending on frequency.

For paths at intermediate $\theta$-values, a different behaviour is observed, although the dispersion in the results is rather large at low frequency. For $\theta \sim 57^\circ$ (Fig. 4b), the curves tend to depart from linearity, with a decay somewhat steeper at low frequency than at high frequency. The *DF/BC* ratio is slightly below that of mean Earth model at low frequency, but becomes significantly lower when $f$ increases. For $\theta \sim 49^\circ$ (Fig. 4c), the most robust feature is the nearly flat section at frequencies higher than 4 Hz. The very sharp decrease at low frequency is marginally significant, as it could be observed for a few records only, because of the short time delay between PKPdf and PKPbc for most of the records of the relevant path (central Asia to PLCA, $\Delta \sim 149.5^\circ$). The shape of the curve is in any case different from that observed for $\theta \sim 57^\circ$ (Fig. 4b) or for $\theta \sim 23^\circ$ (Fig. 4d).

For the most polar paths ($\theta \sim 23^\circ$, Fig. 4d), the curves all reveal a very low *DF/BC* ratio at high frequency (see also the waveforms in Fig. 3b), and again a departure from linearity. The sharp decrease of the *DF/BC* ratio with frequency for polar paths, compared to the mild decrease for equatorial paths, is also clearly apparent on Fig. 3. At 0.4 Hz, *DF/BC* is five times smaller for polar paths than for equatorial paths. It is 25 times smaller at 1.6 Hz, with *DF/BC* as low as 0.016 for polar paths.

In order to check whether this spectacular decrease of *DF/BC* with frequency is a general characteristic of polar paths, or a regional effect, polar paths have been investigated at worldwide scale. They all exhibit similar features [26]. As an example, Fig. 4e shows the result for the path from Kamchatka to QSPA at South Pole, with a turning point beneath New Hebrides.

## 5. Discussion

Two main observations have to be explained. The first one is the now well known anisotropy in attenuation and its correlation to the anisotropy in velocity, with fast paths and strong attenuation in the polar direction. The second and new one is the varying frequency dependence of wave amplitude decay with ray orientation, with a mild linear decay of Ln(*DF/BC*) with frequency for equatorial paths, and a strong, non-linear decay for non-equatorial paths. This results in a very strong anisotropy in wave amplitude at high frequency, with very low DF/BC ratios for polar paths. Also noticeable is the influence of $\theta$ on the spectral shape, observed for paths turning beneath Africa. It will be important in the future to investigate other areas in order to check whether these features are present worldwide, the difficulty being to find favourable geometric configurations of ray paths.

An other important observation is the significant dispersion observed for polar paths. A consequence is that the inner core anisotropic velocity model will depend on frequency, a point to take into account in reconciling eigenmode and body wave models.

It seems unrealistic to ascribe our observations to mantle or to inner core heterogeneities or anisotropy lateral variations [35], even so they may be responsible of part of the scattering in the results. The simultaneous observation of amplitude decay and dispersion is a strong argument in favour of inner core attenuation as the prevailing mechanism.

Previous studies have been able to explain part of our observations with either anelastic attenuation with a specific absorption band [13,17], or scattering by a fabric with specific characteristics [5,7,11,31]. The method used in some previous studies [11,13,17] is based on PKPdf pulse shape modelling, whereas we consider spectral ratio DF/BC, but these two kinds of observations contain potentially the same information. In a model of solidification texturing involving a dendritic growth perpendicular to rotation axis [4], the strong attenuation for polar paths could be explained by the large number of crossed grain boundaries, compared to equatorial paths. By contrast, the mild, linear decay of Ln(*DF/BC*) with $f$ for equatorial paths, which corresponds to a large quality factor ($Q \sim 800$–$1200$), suggests that the contribution of viscous processes to attenuation (if any) is very low. For polar paths, the strong amplitude decrease and the strong dispersion increase observed in the frequency range 0.2–0.5 Hz would correspond to scattering by structures as large as 20–50 km, which seems unrealistically large [7,11]. Other mechanisms will have to be explored [2], related for example to the possible presence of thin fluid sheets between dendrites or along grain boundaries, to melting-freezing in liquid inclusions, to viscous flow between inclusions, or to texturing induced by outer core flow or internal deformation.

## Acknowledgments

I thank the Institutions who provided data for this study through FDSN (CD, G, GE, II, IU GT, PS), and M. Calvet, M. Monnereau, V. Cormier, M. Bergman and two anonymous reviewers of a first version of the manuscript for helpful comments.

## References

[1] J. Aubert, H. Amit, G. Hulot, P. Olson, Thermochemical flows couple the Earth's inner core growth to mantle heterogeneity, Nature 454 (2008) 758–762.
[2] N. Barton, Rock Quality, Seismic velocity, Attenuation and Anisotropy, Taylor and Francis, London, 2007, 729 p.
[3] C. Beghein, J. Trampert, Robust normal mode constraints on inner core anisotropy from model space search, Science 299 (2003) 552–555.
[4] M.I. Bergman, Measurements of elastic anisotropy due to solidification texturing and the implications for the Earth's inner core, Nature 389 (1997) 60–63.
[5] M.I. Bergman, L. Giersch, M. Hinczewski, V. Izzo, Elastic and attenuation anisotropy in directionally solidified (hcp) zinc, and the seismic anisotropy in the Earth's inner core, Phys. Earth Planet. Inter. 117 (2000) 139–151.
[6] J. Bhattacharyya, P. Shearer, G. Masters, Inner core attenuation from short-period PKP(BC) versus PKP(DF) waveforms, Geophys. J. Int. 114 (1993) 1–11.
[7] M. Calvet, L. Margerin, Constraints on grain size and stable iron phases in the uppermost inner core from multiple scattering modelling of seismic velocity and attenuation, Earth Planet. Sci. Lett. 267 (2008) 200–212.
[8] A. Cao, B. Romanowicz, Hemispherical transition of seismic attenuation at the top of the earth's inner core, Earth Planet. Sci. Lett. 228 (2004) 243–253.
[9] V. Cormier, P.G. Richards, Comments on "The damping of core waves" by Antony Qamar and Alfredo Eisenberg, J. Geophys. Res. 81 (1976) 3066–3068.
[10] V.F. Cormier, X. Li, G.L. Choy, Seismic attenuation in the inner core: Viscoelastic or stratigraphic? Geophys. Res. Lett. 25 (1998) 4019–4022.
[11] V.F. Cormier, X. Li, Frequency-dependent seismic attenuation in the inner core 2. A scattering and fabric interpretation, J. Geophys. Res. (2002) 107, doi:10.1029/2002JB001796.
[12] K.C. Creager, Large-scale variations in inner core anisotropy, J. Geophys. Res. 104 (1999) 23127–23139.
[13] D.J. Doornbos, Observable effects of the seismic absorption band in the Earth, Geophys. J. Roy. Astr. Soc. 75 (1983) 693–711.
[14] A.M. Dziewonski, D.J. Anderson, Preliminary reference Earth model, Phys. Earth Planet. Inter. 25 (1981) 297–356.
[15] M. Ishii, A.M. Dziewonski, The innermost inner core of the Earth: Evidence for a change in anisotropic behaviour at the radius of about 300 km, PNSA 99 (2002) 14026–14030.
[16] B.L.N. Kennett, E.R. Engdahl, R. Buland, Constraints on seismic velocities in the Earth from traveltimes, Geophys. J. Int. 122 (1995) 108–124.
[17] X. Li, V.F. Cormier, Frequency dependent seismic attenuation in the inner core 1. A viscoelastic interpretation, J. Geophys. Res. 107 (2002), doi:10.1029/2002JB001795.
[18] H.P. Liu, D.L. Anderson, H. Kanamori, Velocity dispersion due to anelasticity; implications for seismology and mantle composition, Geophys. J. R. Astron. Soc. 47 (1976) 41–58.
[19] D.E. Loper, D.R. Fearn, A seismic model of partially molten inner core, J. Geophys. Res. 88 (1983) 1235–1242.
[20] A. Morelli, A.M. Dziewonski, J.H. Woodhouse, Anisotropy of the inner core inferred from PKIKP travel times, Geophys. Res. Lett. 13 (1986) 1545–1548.
[21] G. Müller, Amplitude studies of core phases, J. Geophys. Res. 78 (1973) 3469–3490.
[22] S.I. Oreshin, L.P. Vinnik, Heterogeneity and anisotropy of seismic attenuation in the inner core, Geophys. Res. Lett. 31 (2004) L02613, doi:10.1029/1003GL018591.
[23] B. Romanowicz, J.J. Durek, Seismological constraints on attenuation in the Earth: a review, in: Karato et al. (Eds.), Earth's deep Interior: Mineral physics and tomography from the atomic to the global scale, AGU Geophysical Monograph 117 (2000) 161–180.
[24] S.C. Singh, M.A.J. Taylor, J.P. Montagner, On the presence of liquid in Earth's inner core, Science 287 (2000) 2471–2474.
[25] A. Souriau, Deep Earth Structure - The Earth's Cores, in : G. Schubert (Ed.), Treatise on Geophysics, Elsevier Ltd, Oxford, 2007, pp. 655–694.
[26] A. Souriau, The frequency dependent anisotropy in attenuation and the structure of the inner core, E.O.S. Trans. AGU (2008), 89 (53), Fall meeting supplement, Abstract DI43A-1756.
[27] A. Souriau, P. Roudil, Attenuation in the uppermost inner core from broadband Geoscope PKP data, Geophys. J. Int. 123 (1995) 572–587.
[28] A. Souriau, B. Romanowicz, Anisotropy in inner core attenuation: a new type of data to constrain the nature of the solid core, Geophys. Res. Lett. 23 (1996) 1–4.
[29] X. Song, D.V. Helmberger, Depth dependence of anisotropy of Earth's inner core, J. Geophys. Res. 100 (1995) 9805–9816.
[30] I. Sumita, P. Olson, A laboratory model for convection in Earth's core driven by a thermally heterogeneous mantle, Science 286 (1999) 1547–1549.
[31] F.E. Stanke, G.S. Kino, A unified theory for elastic wave propagation in polycrystalline materials, J. Acoust. Soc. Am. 75 (1984) 655–682.
[32] S. Tanaka, H. Hamaguchi, Degree one heterogeneity and hemispherical variation of anisotropy in the inner core from PKP(BC)-PKP(DF) times, J. Geophys. Res. 102 (1997) 2925–2938.
[33] J.E. Vidale, P.S. Earle, Fine-scale heterogeneity in the Earth's inner core, Nature 404 (2000) 273–275.
[34] W. Yu, L. Wen, Inner core anisotropy in attenuation, Earth Planet. Sci. Lett. 245 (2006) 581–594.
[35] W. Yu, L. Wen, Complex seismic anisotropy in the Earth's inner core beneath Africa, J. Geophys. Res. 112 (2007) B08304, doi:10.1029/ 2006JB004868.